Relaxation Dynamics of Tryptophan in Water: A UV Fluorescence Up-Conversion and Molecular Dynamics Study

O. Bräm,[†] A. Ajdarzadeh Oskouei,[†] A. Tortschanoff,[†,⊥] F. van Mourik,[†] M. Madrid,[‡] J. Echave,[‡,§] A. Cannizzo,[†] and M. Chergui*[,†]

Laboratoire de Spectroscopie Ultrarapide, Ecole Polytechnique Fédérale de Lausanne, ISIC, SB, Bâtiment CH Station 6, CH-1015 Lausanne, Switzerland, Instituto Nacional de Investigaciones Fisicoquímicas Teóricas y Aplicadas, Universidad Nacional de La Plata, Suc. 4, C.C. 16, 1900 La Plata, Argentina, and Escuela de Ciencia y Tecnología, Campus Miguelete, Edificio Tornavías, Universidad Nacional de San Martín, Martín de Irigoyen 3100, 1650 San Martín, Buenos Aires, Argentina

Received: February 27, 2010; Revised Manuscript Received: June 29, 2010

We report on an ultrafast experimental and simulations study of the early relaxation events of photoexcited tryptophan in water. Experimentally, we used fluorescence up-conversion in both polychromatic and single wavelength detection modes in the 300−480 nm range with polarization dependence. We report on the time evolution of the Stokes shift, bandwidth, and anisotropy from tens of femtoseconds to picoseconds. These observables contain signatures of the simultaneous occurrence of intramolecular and solvent−molecule interactions, which we disentangle with the help of nonequilibrium molecular dynamics simulations. We also observe a breakdown of the linear response approximation to describe our results.

Introduction

Tryptophan (Trp) is the most common amino acid residue in biological systems. Its absorption and emission bands are well separated from the spectral bands of other amino acids and peptides[1] and are very sensitive to the local environment, making it an ideal probe of structural changes in the course of protein functions, folding−unfolding processes, etc.[2,3] Indeed, several of its fluorescence features such as band maximum and width,[4] quantum yield,[5] lifetimes,[6] energy transfer,[7] and time-resolved anisotropy[8] have been extensively exploited with this aim. Fluorescence up-conversion studies on Trp were carried out to probe the solvation dynamics at the surface of[9−13] or within[14] proteins. More recently, ultrafast UV transient absorption spectroscopy was used to probe the Trp response to a light triggered biological function in bacteriorhodopsin,[15,16] and in hemoproteins.[17,18] As part of our strategy to use Trp residues as local probes of protein dynamics, we recently implemented femtosecond UV photon echo peak shift experiments,[19−21] and UV femtosecond fluorescence up-conversion experiments, with broad band detection.[22] Noteworthy both setups use excitation pulses with a width of 4 nm in the 260−300 nm range, allowing us to selectively excite only Trp and not the other aromatic amino acid as tyrosine.

The photophysics of Trp is rather complex. The first LUMO states ^1L_a and ^1L_b are nearly degenerate and have different static dipole moments.[3] Due to its larger dipole moment, the ^1L_a state has lower energy than the ^1L_b state and is considered to be the emitting state in most polar environments. The ^1L_b state was reported to relax to the ^1L_a state in less than 100 fs.[4,23] In bulk water, the presence of different rotamers due to the different relative orientations of amino- and carboxylic groups, results in two different radiative time constants: a main 3 ns component with a smaller and faster component of 0.5 ns, the latter having a slightly different spectrum centered at 335 nm.[24] In the 0−100 ps temporal window, only $^1L_b \rightarrow {}^1L_a$ internal conversion (IC) and solvation dynamics occur together with rotational diffusion.[1] Ultrafast time-resolved Stokes shift (TRSS) measurements on tryptophan were carried out to extract the local solvation dynamics by characterizing the solvation correlation function. Shen and Knutson,[8] Zewail and co-workers,[9−12,14,25] and Zhong and co-workers[13,23] measured single-wavelength fluorescence traces across the spectrum of aqueous Trp. Zhong et al. established a procedure to reconstruct the emission spectrum and found a total Stokes shift up to the longest time delay (830 ps) of 2186 cm^{-1}, including a 200 cm^{-1} shift in the nanosecond time domain, attributed to rotamer dynamics. They fitted their correlation function with a Gaussian-type component and an exponential decay and obtained two decay times of 340 fs and 1.6 ps, in agreement with the water solvation time constants.[26,27] Interestingly a simple analysis of steady-state absorption and emission spectra of aqueous Trp would give a total expected Stokes shift of ∼3800 cm^{-1} (see later), implying that a shift of ∼1600−1700 cm^{-1} occurs on a time scale shorter than their temporal resolution (∼400 fs). A similar effect was predicted by Callis et al. who, on the basis of molecular dynamics simulations, found that 2000 cm^{-1} of the shift would occur within 20 fs, with significant contribution from 20 water molecules within 6 Å of the indole ring center.[3] The occurrence of Stokes shift in tens of femtoseconds has been recently confirmed by experimental studies on metal complexes and on organic dyes, where "instantaneous" Stokes shifts as large as 6000 cm^{-1} are observed between excitation and emission.[28−32] In these cases, internal vibrational redistribution (IVR) and internal conversion (IC) on subvibrational time scales seem the most likely origin of the effect.[33]

Since the ^1L_a and ^1L_b sates are characterized by transition dipole moments with almost perpendicular orientations, time-resolved anisotropy measurements were used,[8,23,34,35] concluding that the internal conversion (IC) time τ_{IC} is <100 fs. These

[†] Ecole Polytechnique Fédérale de Lausanne.
[‡] Universidad Nacional de La Plata.
[§] Universidad Nacional de San Martín.
[⊥] Current address: CTR Carinthian Tech Research AG, Europastrasse, 4/1, 9524 Villach/St. Magdalen, Austria.

10.1021/jp101778u
Published on Web 08/10/2010

studies were carried out with a typical temporal resolution of ≥300 fs, using a monochromatic detection (i.e., single wavelength detected fluorescence kinetics). The use of a polychromatic detection in the UV[20,22] is important to separate the spectral evolution due to the IC process from other mechanisms, such as cooling and solvation dynamics. Furthermore, this detection makes the correction for group velocity dispersion (GVD) more reliable, since it can easily be estimated with independent measurements on dye laser emission[22] or with a continuum.[31]

As a preliminary study of the Trp response in biological systems, we report here on an ultrafast UV broad-band fluorescence study of aqueous Trp at pH 7, aimed at characterizing and describing in detail the initial IC dynamics and early intra- and intermolecular response. We use a polychromatic detection with 180 fs time resolution, detecting the time-resolved fluorescence with parallel and orthogonal polarization. The observed signals are compared with nonequilibrium MD simulations, providing a convincing picture of the early dynamics of Trp in bulk water.

Materials and Methods

Fluorescence Detection Scheme. The fluorescence up-conversion setup has already been described in detail elsewhere[22,31] Briefly, we use 290 nm pulses with a bandwidth of about 4 nm and a pulse width of about 70 fs at a repetition rate of 130 kHz. The UV-excited emission from the sample is filtered with a 300 nm cutoff filter to remove the remaining excitation light, and then mixed in a BBO crystal with the 800 nm gate beam. The up-converted signal is detected with a monochromator equipped with a CCD camera. To overcome the phase-matching condition of the sum frequency (SF) crystal, the latter is continuously turned during the measurement. Since we use a type I sum-frequency process, our detection is intrinsically polarization selective such that a parallel and orthogonal detection scheme was achieved by placing a half-wave-plate in front of the UV beam before excitation. A partial depolarization is expected due to the presence of parabolic mirrors used to focus the emitted light into the SF crystal. To estimate the instrumental polarization contrast, we measured the instantaneous anisotropy value of the Raman line of water obtaining a value of 0.55, close to the expected 0.63.[36] To take this depolarization into account, we will correct the experimental data by scaling them by a factor of 1.15 (= 0.63/0.55). The broad-band measurements were carried out with a 250 μm BBO, providing a time resolution of 180 fs as determined by a measurement of the Raman response from the solvent (Figure S1, Supporting Information). Kinetic traces up to 600 fs were acquired with a thinner BBO crystal of 100 μm at 305, 310, 315, 325, 335, 365, and 380 nm, achieving a temporal resolution of 120 fs. In all measurements, the solution was circulated inside a 0.2-mm-thick quartz flow cell.

The sample consisted of 130 mg of Trp molecules (from Alfa Aesar) dissolved in 250 mL of buffer at pH = 7, giving a concentration of 2.55 mM, and a corresponding optical density of 0.2 OD at 290 nm. Reabsorption of fluorescence is negligible (<0.02 OD for λ >300 nm). The Trp molecules were excited by 23 nJ pulses and the proportion of excited-state molecules in the excited volume is estimated to be around 8%. The linearity of the signal with the excitation power was verified before measurements. To avoid photodegradation, the sample flow and repetition rate were chosen to achieve one shot per spot. Moreover, the signal intensity was the same during the acquisition time and no change in the absorption spectrum was observed after the measurement. The sample was at room temperature (~20 °C). Before analyzing the time-resolved fluorescence spectrum, the Raman line of water was carefully removed from the data, using a Gaussian fit of the up-converted Raman band in pure water (Figure S1B, Supporting Information).

Data analysis is performed in terms of spectral moments, with the zero- (M_0, total area), first- (M_1, average spectral position), and second-order (M_2, spectral variance) moments being extracted from the data. The anisotropy is derived from the zero moment of the parallel and orthogonal component:

$$r_{tot}(t) = \frac{M_0^{||}(t) - M_0^{\perp}(t)}{M_0^{||}(t) + 2 \cdot M_0^{\perp}(t)} \quad (1)$$

and the spectrally resolved anisotropy is derived from the expression

$$r_{tot}(\nu,t) = \frac{I_{||}(\nu,t) - I_{\perp}(\nu,t)}{I_{||}(\nu,t) + 2 \cdot I_{\perp}(\nu,t)} \quad (2)$$

where ν and t stand for the wavenumber and time variables and $I_{||}$ and $I_{\perp}$ are the parallel and orthogonal components of the intensity, respectively. It is important to stress that we measured parallel and orthogonal components one after the other without any change in the setup to avoid any artifact due to relative time zero indetermination. The absolute time zero value was extracted by a simultaneous fit of $M_0^{||}$ and $M_0^{\perp}$. For the single-wavelength time traces, to be sure of the relative amplitudes, the longest time (600 fs) spectrum was reconstructed and scaled with respect to the one from broad-band detection at the same time. The same moment analysis is then performed before deriving the anisotropy. For all values reported here, the error corresponds to twice the standard deviation.

Nonequilibrium Molecular Dynamics Simulations. Simulations were run using Trp in its neutral zwitterionic form (which is dominant at pH = 7) placed in a cubic box with sides of 3 nm length, surrounded by 882 water molecules. Periodic boundary conditions were applied. Classical trajectories were calculated using the program package GROMACS.[37] We used the GROMOS96 force field and the SCP/E water model, which was previously used to study Trp in water,[38,39] a Lys-Trp-Lys tripeptide[40] and Trp in apomyoglobin.[41] A cutoff of 0.9 nm was used to produce the nonbonded pair list. Similarly, we used 0.9 nm as a cutoff for the calculation of the van der Waals interactions and short-range electrostatic interactions and the particle mesh Ewald algorithm[42,43] (PME) was used to deal with the long-range interactions. We constrained bond lengths using LINCS,[44] which allowed the use of a 2 fs time step.

The S_0 ground state of Trp was modeled using the GROMOS96 parameters, including atom charges. The ^1L_a excited electronic state was modeled as having exactly the same parameters (equilibrium bond distances, force constants, etc.) as the ground state, but different site charges. These charges were obtained by adding the charge differences obtained in the ab initio calculations of ref 45 to the ground-state partial charges of the GROMOS96 force-field, following previous work.[40,46] We used a similar procedure to simulate the ^1L_b excited state. Basically, the simulation assumes that the equilibrium structure of the indole group is the same in the two excited states as in the ground state. In this way, the simulations give information

on the spectral evolution due mostly to solvent relaxation. Its drawback is an underestimation of the spectral widths.

Equilibrium ground-state simulations were run in the *NVT* ensemble. A constant temperature of 295 K was maintained by coupling the system to a Berendsen thermostat.[47] First the system was equilibrated by starting with energy minimization followed by an equilibration run of 0.5 ns. The production of a 10 ns trajectory was obtained. In a similar way, using the partial charges of the excited Trp, we obtained 10 ns equilibrium trajectories for the ^1L_a and ^1L_b excited electronic states. The time-dependent fluorescence process for ^1L_a (^1L_b) was simulated as follows: 500 initial conditions were obtained from the ground-state trajectory by picking one configuration every 20 ps, which is a time long enough to consider these configurations as independent. Each configuration was used in a new 10 ps simulation obtained using the ^1L_a (^1L_b) potential. In this way, we obtained 500 excited-state trajectories each 10 ps long for ^1L_a (^1L_b). The excited-state trajectories were run using the *NVE* ensemble, to avoid artifacts due to temperature coupling.

For a given configuration of the system, the energy difference between an excited electronic state and the ground state can be written

$$\Delta E = E_e - E_g = \nu_0 + \Delta E^{IT} + \Delta E^{TS} \quad (3)$$

where ΔE^{IT} is the difference between the excited and ground state of the electrostatic interactions between the indole and the Trp charged groups (mainly NH^{3+} and COO^-) (IT stands for intra-tryptophan), ΔE^{TS} is the difference in electrostatic interactions between the indole charges and water (TS stands for tryptophan-solvent), and ν_0 is the difference between the minima of the excited-state and ground-state potentials in vacuum. Actually, the value of the latter cannot be obtained by this type of calculation that gives information only on shifts relative to this frequency. For convenience, we use as energy reference the equilibrium average $\Delta E \leftarrow \Delta E - \langle \Delta E \rangle_{e,\infty}$. For each excited state, using the 500 nonequilibrium trajectories we obtained at each time-step the histogram of energy differences, which represents the emission spectrum. This spectrum was characterized in a similar way as the experimental one, by calculating the time-dependent average frequency (Stokes shift) and standard deviation (bandwidth). For the shift we have, explicitly

$$\Delta\nu(t) = \frac{\langle \Delta E \rangle_{e,t} - \langle \Delta E \rangle_{e,\infty}}{h} \quad (4)$$

where the notation "e,*t*" stands for averaging over the excited-state ensemble at time *t*. To simulate the effect of the 180 fs experimental instrumental response for broad band detection, we also obtained spectra by convoluting the simulated spectrum with a Gaussian of 180 fs fwhm.

Results and Discussion

Anisotropy. Parts A and B of Figure 1 show time-wavelength plots of the fluorescence of tryptophan in water, in the first 5 ps for parallel and orthogonal detection. We detect a broad emission from 300 to 450 nm, which shifts to lower energies in the first picosecond. We construct the time−energy plot of the anisotropy according to eqs 1 and 2 (Figure 1C), which shows a spectral dependence at time zero in the range 26 000−32 000 cm^{-1} that disappears within the pulse width (Figure 1D). Figure 2 reports the anisotropy as a function of

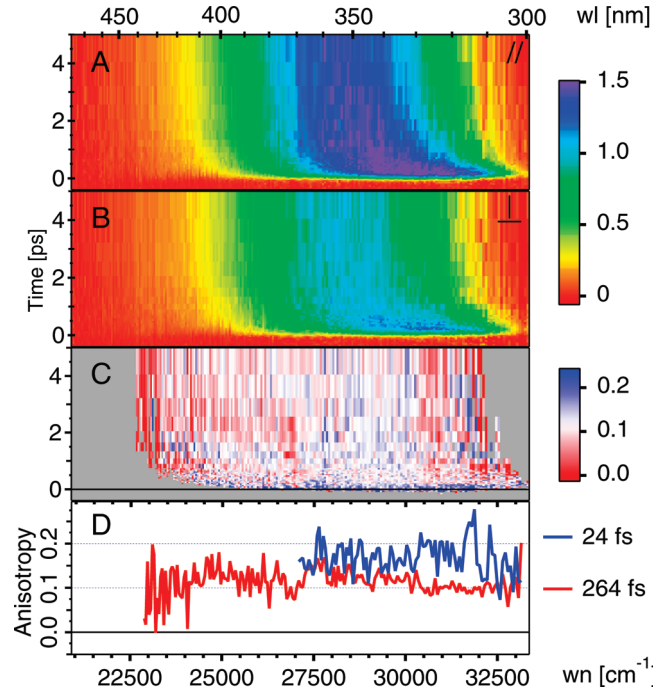

Figure 1. Time−wavenumber plots of time-resolved fluorescence spectrum of tryptophan in water, in the first 5 ps, with parallel (panel A) and orthogonal (panel B) polarization. (C) Time−wavenumber plot of the anisotropy over the first 5 ps. The black horizontal line corresponds to the time zero. [Intensity is color coded accordingly to the legend on the right side]. Selected anisotropy spectra are depicted on panel D, at 24 and 264 fs.

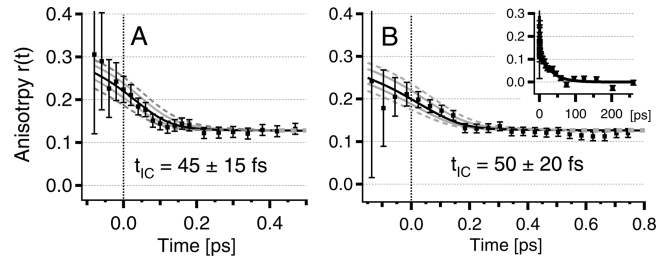

Figure 2. (A) Time-resolved anisotropy from the frequency-integrated fluorescence reconstructed from the set of kinetic traces across the spectrum acquired with an irf (instrumental response function) width of 120 fs. (B) Time-resolved anisotropy from the frequency-integrated fluorescence of Figure 1A,B (irf width of 180 fs). The inset shows the total probed range up to 260 ps. Black dots are the data with error bars, and the black line is the best fit. The corresponding τ_{IC} and uncertainty $\Delta\tau_{IC}$ are reported. The gray solid (dashed) lines show the fit function corresponding to $\tau_{IC} \pm \Delta\tau_{IC}$ ($\tau_{IC} \pm 2\cdot\Delta\tau_{IC}$).

time obtained from both broad-band and single-wavelength detected fluorescence signal, the latter having a better temporal resolution (120 fs). A maximum value of 0.25 is found, which decays in less than 200 fs to 0.13 and finally vanishes on a time scale of tens of picoseconds. The latter is due to rotational diffusion and, by fitting the 250 ps range with an exponential decay, we find a rotational diffusion time of 34 ± 4 ps, in agreement with the literature.[8,23,40,46] Concerning the ultrafast dynamics, the expected time-zero anisotropy value is 0.4, and the smaller value found here speaks for dynamics faster than our time resolution. This is indeed the case, as derived in ref 14 (<80 fs), which reported an anisotropy close to 0.4, due to $^1L_b \rightarrow {}^1L_a$ IC. To estimate more precisely the IC time, we model it in terms of the time-dependent population of both states. We assume that for both ^1L_a and ^1L_b states, the transition dipole moment of excitation is collinear to the emission one. At time

TABLE 1: Parameters Resulting from the Fit on Data in Figure 2A[a]

	n_a^0	α^{15}	$2(\ln 2)^{1/2}\cdot\sigma_{irf}$ (fs)	τ_{L_a} (ns)	τ_{rot} (ps)	τ_{IC} (fs)
value	0.55	0.455	180	3	34	45
uncertainty	±0.01	fixed	fixed	fixed	±8	±10

[a] Fraction of initially excited tryptophan in the ^1L_a state, n_a^0; ratio between ^1L_a and ^1L_b transition dipole moments, α; FWHM irf, $2(\ln 2)^{1/2}\cdot\sigma_{irf}$; ^1L_a fluorescence decay time, τ_{L_a}; rotational diffusion time constant, τ_{rot}; IC time constant, τ_{IC}.

zero, we excite a mixture of molecules in the ^1L_a and ^1L_b state. The latter will undergo internal conversion to the ^1L_a state in less than 100 fs while the former will undergo solvation dynamics and rotational diffusion on longer time scales. Defining $n_a(t)$ and $n_b(t)$ as the respective populations of ^1L_a and ^1L_b states at time t, and μ_a and μ_b as the respective emission transition dipole moments, one can write the following set of equations, assuming a Gaussian instrumental response function (irf) with width σ_{irf}:

$$\begin{aligned} n_a(t) &= [n_a^0\cdot e^{-t/\tau_{L_a}}] \odot e^{-[(t-t_0)/\sigma_{irf}]^2} \\ n_b(t) &= [n_b^0\cdot e^{-t(1/\tau_{IC})}] \odot e^{-[(t-t_0)/\sigma_{irf}]^2} \\ n_{ba}(t) &= [n_b^0 - n_b^0\cdot e^{-t(1/\tau_{IC})}] \odot e^{-[(t-t_0)/\sigma_{irf}]^2} \end{aligned} \quad (5)$$

n_a^0 and n_b^0 being, respectively, the populations of the ^1L_a and ^1L_b states excited at time zero (t_0), n_{ba} being the population of molecules in the ^1L_a state stemming from the IC (initially in the ^1L_b state), τ_{IC} is the IC time constant, and τ_{L_a} is the lifetime of ^1L_a state. Knowing the time-dependent dipole moments through the time-dependent populations, it is straightforward to find their contributions to the parallel and orthogonal intensities, and thus to derive the anisotropy expression:

$$\begin{cases} I_z = \left(\frac{\mu^2}{5}\right)\left[(n_a(t) + \alpha^2 n_b(t))\cdot\left(\frac{5}{3} + \frac{4}{3}e^{-t/\tau_{rot}}\right) + n_{ba}(t)\cdot\left(\frac{5}{3} - \frac{2}{3}e^{-t/\tau_{rot}}\right)\right] \\ I_x = \left(\frac{\mu^2}{5}\right)\left[(n_a(t) + \alpha^2 n_b(t))\cdot\left(\frac{5}{3} - \frac{2}{3}e^{-t/\tau_{rot}}\right) + n_{ba}(t)\cdot\left(\frac{5}{3} + \frac{1}{3}e^{-t/\tau_{rot}}\right)\right] \end{cases}$$

$$\Rightarrow r = \frac{2(n_a + \alpha^2 n_b(t)) - n_{ba}(t)}{5[n_a + \alpha^2 n_b(t) + n_{ba}(t)]}\cdot e^{-t/\tau_{rot}} \quad (6)$$

where $\alpha = \mu_b/\mu_a$ (μ_a and μ_b are known from experimental and theoretical results[15]) and τ_{rot} is the rotational diffusion time constant.

According to eqs 5 and 6 the 0.13 value at 0.5 ps (see Figure 2), after IC is finished and rotational dynamics are still negligible ($\tau_{rot} = 34$ ps), is a direct measurement of the ratio of initial ^1L_a and ^1L_b populations. We estimate the percentage of the ^1L_b (^1L_a) population to be around 45% (55%), in agreement with the relative absorption intensity of both states.[8] The solid lines in Figure 2 are the best fits based on eqs 5 and 6, with the corresponding parameters given in Table 1. The agreement with experimental data in the temporal region of the internal conversion is excellent. This is even more remarkable since, to describe the dynamics, the IC time constant is the only free important parameter, while all other parameters (n_a^0, α, τ_{rot}, τ_{L_a}, σ_{irf}) are unequivocally determined by the experimental values at longer time or by independent measurements. We find $\tau_{IC} = 50 \pm 20$ and 45 ± 15 fs, from the analysis of broad-band and single-wavelength detected measurements, respectively. These values and their relative uncertainties are supported by the comparison of the experimental data with the curves corresponding to the upper and lower value of τ_{IC} ($\tau_{IC} \pm \Delta\tau_{IC}$). These curves are indeed just within the error bars, and considering $\tau_{IC} \pm 2\cdot\Delta\tau_{IC}$, we obtain unsatisfactory curves (Figure 2).

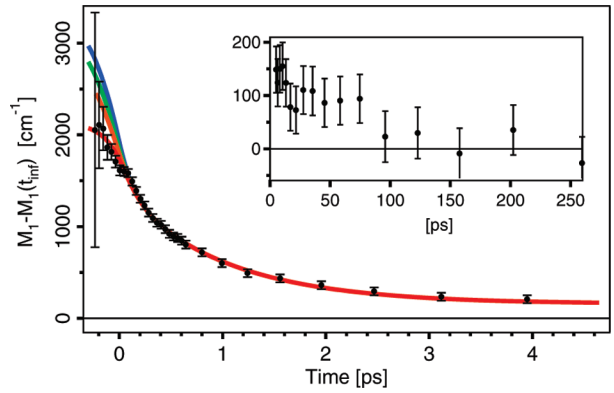

Figure 3. Emission frequency shift (difference between the first spectral moment and its long time value (for $t > 200$ ps)) of the Trp emission band (black dots). The solid red curve shows the best fit according to eq 10, (see text). Orange, green, and blue solid curves are the same function with an additional exponential component with 1700 cm^{-1} amplitude and, 10, 20, and 30 fs time constant, respectively. The inset shows the first spectral moment on a 250 ps temporal window.

Figure 1C shows the time−energy plot of the anisotropy over the first 5 ps. On this plot, one can clearly distinguish at time zero, a broad band between 28 000 and 32 000 cm^{-1}. This spectral dependence can be appreciated by comparing the anisotropy spectra close to time zero and after the IC at 260 fs, on the panel D of Figure 1, and is indeed the signature of the ^1L_b emission band prior to IC. More information on earliest dynamics (IC dynamics) will be obtained by analysis of spectral width kinetic, reported in the following paragraphs.

Solvation and Intramolecular Dynamics. From the parallel and orthogonal components of the fluorescence intensity, we reconstruct the intensity as measured at magic angle (data not shown), i.e., free from rotational diffusion, according to

$$I(\nu,t) = \frac{1}{3}[I_{||}(\nu,t) + 2\cdot I_{\perp}(\nu,t)] \quad (7)$$

From these data, we calculate the spectral moments. M_0 shows an instantaneous rise followed by a weak and long decay over the observed 250 ps (data not shown), which we tentatively assign to the 0.5 ns decay component related to Trp rotamer dynamics.[24] M_1 (Figure 3) exhibits a remarkable Stokes shift of 2000 cm^{-1} complete in 10 ps. In the 10−260 ps range (Figure 3, inset), one can see a 100 cm^{-1} red shift due to the 0.5 ns radiative decay component, which has an associated spectrum slightly blue-shifted with respect to the steady-state spectrum.[24]

To derive a suitable fit function, we observe that in the case of an impulsively excited fluorescence band $I_\delta(\nu,t)$ the first moment is

$$M_1^\delta(t) = \frac{m_1^\delta(t)}{M_0^\delta(t)} \quad \text{with} \quad m_1^\delta(t) = \int \nu\cdot I^\delta(\nu,t)\cdot d\nu \quad (8)$$

but the experimental signal (Figure 3) is affected by a finite IRF according to

$$M_1(t) = \frac{(m_1^{\delta} \odot \mathrm{irf})(t)}{(M_0^{\delta} \odot \mathrm{irf})(t)} \tag{9}$$

In the case of multiexponential decay of the first spectral moment, we obtain

$$M_1(t) = \frac{\sum_i M_1^i \cdot \mathrm{erfex}(\sigma_{\mathrm{irf}}, t_0, \tau_i, t)}{\mathrm{erfex}(\sigma_{\mathrm{irf}}, t_0, \tau_{L_a}, t)} \tag{10}$$

where t_0 is the time zero and M_i and τ_i are the amplitude and time constants of the ith exponential contribution. For the sake of clarity we have defined

$$\mathrm{erfex}(\sigma_{\mathrm{irf}}, t_0, \tau_i, t) = (e^{(-t/\tau_i)} \cdot u(t_0, t)) \odot e^{-[(t-t_0)/\sigma_{\mathrm{irf}}]^2} \tag{11}$$

which describes the convolution of an exponential decay starting at t_0 ($u(t_0,t)$ is a step function centered at t_0) with the Gaussian irf.

One should note that the fitting function is no longer a simple linear combination of exponential decays. On a time scale comparable with the irf, the erfex denominator makes the function diverge from the multiexponential decay behavior. The only free parameters involved in this fit are the different time constants and their associated amplitudes.

We fitted eq 10 with two exponential components, in the 0−10 ps range, and the result is plotted in Figure 3. The resulting time scales with their respective amplitude are summarized in Table 2. We obtain relaxation times (amplitudes) of 160 ± 40 fs (720 ± 110 cm^{-1}) and 1.02 ± 0.12 ps (1330 ± 120 cm^{-1}), corresponding to a total shift of 2050 cm^{-1}. A mirror image of the Trp absorption band yields an emission spectrum centered at ∼32 000 cm^{-1}. This value is in good agreement with measurement of Trp emission spectrum in glassy matrices at cryogenic temperature.[48] Indeed, this would correspond to the exact spectrum of Trp surrounded by an unrelaxed solvent. Compared to the steady-state emission centered at 28 200 cm^{-1} (355 nm), this gives a total expected Stokes shift of ∼3800 cm^{-1}, implying that a shift of 1700−1800 cm^{-1} has occurred on a time scale within our temporal resolution, as already supported by Callis et al.[3] and confirmed by our MD simulations (see below). In Figure 3, the resulting fitting function with the same parameters is plotted, with an additional ultrafast exponential component having an amplitude of 1700 cm^{-1}: a relevant discrepancy of the curve is observable for decay constants longer than 10 fs. The orange curve of Figure 3 (10 fs additional component) characterizes the most acceptable discrepancy from the data and gives an upper limit of 10 fs to the time scale of this dynamics.

Concerning the width of the emission band, the square root of the variance has also been computed (Figure 4), showing a fast rise in a few tens of femtoseconds corresponding to a broadening of 500 cm^{-1} followed by a biexponential decay of 0.5 and 7 ps over which the width decreases by 180 cm^{-1}. This behavior can be observed by directly comparing the shapes of normalized spectra at different times (inset of Figure 4). The two slowest time scales do not agree with water solvation times found by M_1 analysis, indicating that these dynamics are not solvation driven. We tentatively assign them to vibrational cooling. Concerning the fastest component, it is so fast that we can exclude also cooling dynamics, signifying an intramolecular origin. In particular, it can be explained as a signature of IC process on the profile of the emission band. We consider that due to their different permanent dipole moments, the ^1L_a and ^1L_b states generate emission bands at different wavelengths. We can model the overall emission as the sum of two different spectral components each with its own spectral profile ($g_1(\nu,t)$ and $g_2(\nu,t)$). The IC process will induce a time-dependent profile as described by the following equations:

$$\begin{aligned} g(\nu,t) &= \alpha(t) \cdot g_1(\nu) + [1 - \alpha(t)] \cdot g_2(\nu) \\ \langle \nu \rangle &= \alpha(t) \langle \nu \rangle_1 + (1 - \alpha(t)) \langle \nu \rangle_2 \\ \sigma^2 &= \alpha(t) \sigma_1^{\,2} + (1 - \alpha(t)) \sigma_2^{\,2} + \\ &\quad \alpha(t)(1 - \alpha(t)) |\langle \nu \rangle_1 - \langle \nu \rangle_2|^2 \end{aligned} \tag{12}$$

where $g(\nu,t)$ is the total emission profile with first moment $\langle \nu \rangle$ and variance σ^2 (the indices 1 and 2 refer to the respective single components) and $\alpha(t)$ takes into account the IC from ^1L_b to ^1L_a states. Figure 5 shows the kinetic model described above for some indicative but meaningful values, corroborating the idea that the fast rise observed stems from the difference in the ^1L_a and ^1L_b emission spectra, and only to a lower extent to IVR. To take into account the decay following the rise, experimentally observed on longer times, we should just include cooling narrowing assuming time-dependent σ_2 ($\sigma_2(t) = \sigma_2^{\max} - 150(1 - e^{t/\tau_{\mathrm{cooling}}})$).

Nonequilibrium Molecular Dynamics Simulations. The time-dependent fluorescence of Trp in different environments

TABLE 2: Exponential Decay Times with Their Respective Pre-exponential Factor in Parentheses from the Best Fit of M_1 and Square Root of M_2 of the Experimental and MD Simulations Data, Negative Amplitude Indicating a Rising Component

	experiment		MD simulation	
	time constant (ps)	amplitude (cm^{-1})	time constant (ps)	amplitude (cm^{-1})
M_1			0.009 ± 0.001	1250 ± 50
	0.16 ± 0.04	720 ± 100	0.175 ± 0.007	1560 ± 30
	1.02 ± 0.12	1330 ± 120	1.20 ± 0.024	950 ± 20
$M_2^{1/2}$	0.05 ± 0.01	500 ± 100	0.060 ± 0.015	−140 ± 20
	0.5 ± 0.2	100 ± 20	0.930 ± 0.07	170 ± 10
	7.5 ± 3.3	80 ± 20		

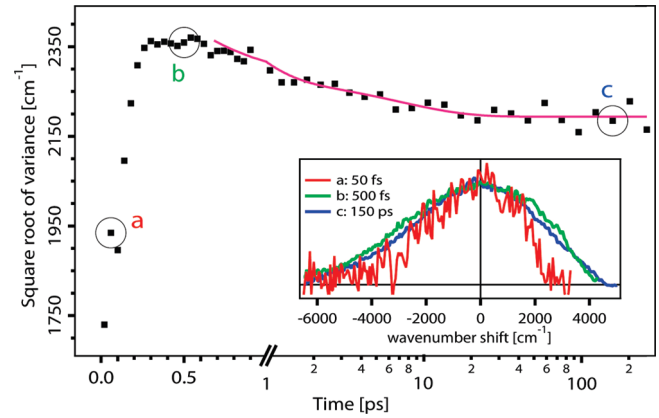

Figure 4. Square root of the variance (standard deviation) of the Trp emission spectrum. The solid red line is the best fit in terms of biexponential decay. The inset shows normalized spectra at the three characteristic times as marked on the main graph at 50 fs (a), 500 fs (b), and 150 ps (c). The spectra have been shifted to zero to better compare the spectral shape differences.

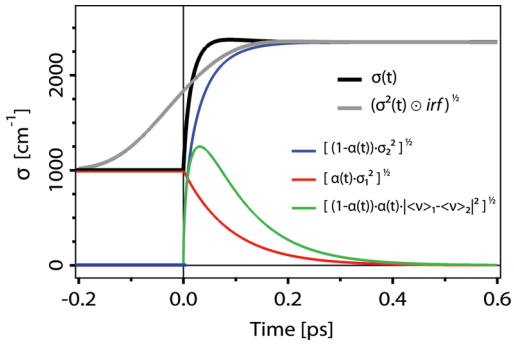

Figure 5. Square root of the variance kinetics model (black), using eqs 12 and assuming $\sigma_1 = 1000$ cm^{-1}, $\sigma_2 = 2350$ cm^{-1}, a 2500 cm^{-1} separation between the two spectra (indicative values), and an IC time of 45 fs from an initial condition of equally populated ^1L_a and ^1L_b states. The blue, red, and green lines show respectively the first, second, and third terms of the contributions to σ^2 in eqs 12. The gray line shows this function convoluted with the irf.

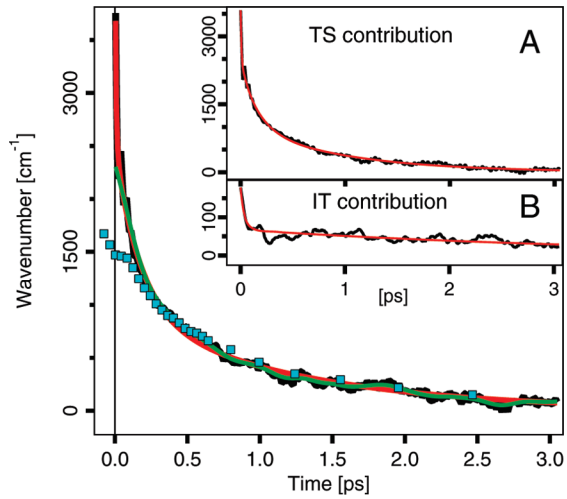

Figure 6. Experimental average emission frequency (first spectral moment) of the ^1L_a emission band (blue square dots) along with the fit (red solid line) and convolution with instrumental response (solid green line) of the computed average emission frequency (black solid line). Inset A reports the tryptophan-solvent contribution with its best fit (red solid line). Inset B reports the tryptophan-tryptophan contribution with its best fit (red solid line).

has been the subject of several theoretical investigations.[3,4,40,46,49] Most studies assumed the validity of the linear response approximation (LRA), which relates the time-dependent Stokes shift to the autocorrelation function of the energy difference in the ground (or excited) state. A recent study applied the LRA to separate the water and protein contributions to the time-dependent Stokes shift of Trp in the protein monellin and Trp in water.[46] Also, nonequilibrium molecular dynamics simulations were performed on a Trp in a tripeptide[40] and apomyoglobin.[41] These simulations can separate the different contributions to the fluorescence dynamics and help interpret the experimental results.

Using nonequilibrium simulations, we obtained time-dependent emission spectra for the excited electronic states ^1L_a and ^1L_b. The ^1L_a and ^1L_b simulated emission spectra are shown in Figure S2 (Supporting Information), along with the calculated first moment, whereas Figure S3 (Supporting Information) shows their respective square root of variance. The spectrum for ^1L_b is qualitatively similar, but much narrower, and the Stokes shift ($\sim$20 cm^{-1}) is negligible in comparison to that of ^1L_a. Noteworthy, these spectral evolutions are mostly due to solvent relaxation as previously discussed. The underestimation of the spectral widths and the impossibility to estimate the frequency for the gas-phase 0−0 transitions make unfeasible the combination of ^1L_a and ^1L_b theoretical spectra to be compared with experimental spectral profiles. However, even if the spectra cannot be combined, since the ^1L_b state is very short-lived ($\tau_{IC} \sim 45$ fs), beyond the first 100 fs, we are left with ^1L_a as the only emitting state. This, together with the fact that the experimental temporal response is 180 fs and that more than 50% of the molecules are directly excited to ^1L_a, allows us to consider the experimental spectrum at magic angle to be mainly due to ^1L_a, at least after the first 100 fs.

For a more detailed analysis, we calculate the first and second moments of the spectra. Figure 6 shows the average frequency for the simulated ^1L_a spectrum. The reference is the frequency averaged over the interval that goes from 9 to 10 ps. We fit the time-dependent profile using three exponentials (Figure 6) covering a shift of $\sim$3750 cm^{-1} after excitation: a large rapid shift with a time constant (amplitudes) of 9 fs (1250 cm^{-1}), followed by further shifts with time constants 175 fs (1560 cm^{-1}) and 1.2 ps (950 cm^{-1}). For ^1L_a we have a total (static) Stokes shift of $\sim$3870 cm^{-1}, calculated using the equilibrium ground- and excited-state trajectories. Therefore, after the initial 10 ps there is a further shift to the red of $\sim$100 cm^{-1}, which is probably due to re-equilibration of the Trp rotamers, occurring on the nanosecond time scale. We find an excellent agreement of the time zero value with the expected total Stokes shift and of the 9 fs time constant with the experimentally determined 10 fs upper limit. The other two relaxation times agree with previous work[50] and are in very good agreement with the values of 160 fs and 1.02 ps obtained in the present experiments, whose assignment is discussed below. This confirms the validity of the assumption that the observed spectral behavior is mainly taken into account by the ^1L_a dynamics, even at the earliest times. In particular, it proves that the origin of the "instantaneous" Stokes shift is mostly related to the effect of solvent inertial response[27,49] on the ^1L_a state. The main difference between the theoretical (3760 cm^{-1}) and experimental (2050 cm^{-1}) Stokes shift is accounted for by convolution of the simulated spectra with a Gaussian irf (instrumental response function) of 180 fs fwhm, which yields a Stokes shift of $\sim$2300 cm^{-1} (green trace in Figure 6).

To further analyze the processes underlying the frequency shift, it is instructive to separate it into intra-tryptophan (IT) and tryptophan-solvent (TS) contributions, which can be done in the simulations since the Coulomb energy is additive. Indeed, even if the adopted simulation approach excludes IT contribution due to structural rearrangement, we have IT consisting of the interaction between the Trp partial charges. The IT contribution to the static Stokes shift is 214 cm^{-1} while the TS contribution is 3655 cm^{-1}, i.e., 5.5% and 94.5%, respectively, of the overall static Stokes shift, in good agreement with previous work that used a different water model.[46] In Figure 6 we show the time−frequency plots corresponding to the TS (panel A) and IT (panel B) contributions. The TS contribution is adequately fitted ($R = 0.99$) using three exponentials with relaxation times (amplitudes) of 8 fs (1134 cm^{-1}), 154 fs (1397 cm^{-1}), and 0.95 ps (1045 cm^{-1}). The IT contribution can be fitted with two exponentials of relaxation times 37 fs (110 cm^{-1}) and 3.6 ps (68 cm^{-1}). As expected, the fit to the total Stokes shift discussed previously only shows the relaxation times due to solvent relaxation. We will see next, however, that the experimental methodology here adopted will allow us to study the dynamics of internal (IT) motions analyzing the bandwidths.

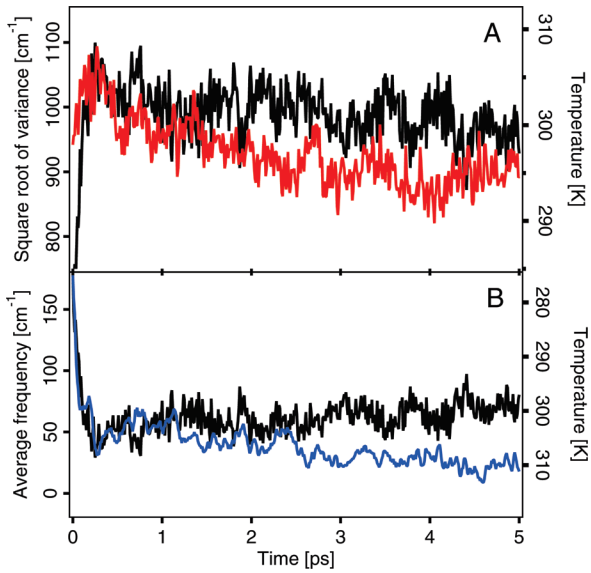

Figure 7. (A) Square root of the variance of the emission band (red) compared to local temperature of Trp (black). (B) IT contribution to the average frequency of the emission band (blue) from Figure 6B compared to the local temperature of Trp (black). The temperature scale of panel B is inverted with respect to that of panel A for a better comparison.

We calculate the second moment of the simulated spectra, which for the ^1L_b state is small (~60 cm^{-1}) and constant. However, as shown in Figure 7A (red trace), the second moment of the simulated ^1L_a spectrum is time-dependent, with an initial rise of ~140 cm^{-1} followed by a decrease of ~170 cm^{-1} with lifetime of ~1 ps. This decrease is in accordance with the narrowing of the experimental emission band occurring in 0.5 ps and attributed to vibrational cooling (Figure 4 and Table 2). The fast rise would speak for an increase of Trp temperature and therefore for an IVR mechanism in the first tens of femtoseconds. However, the initial rise disappears when the spectrum is convoluted with a Gaussian of 180 fs fwhm, so that it will be missed in the experiment. This confirms that the initial rise of the experimental spectrum is due to IC rather than IVR. We should note here that the simulated bands are much narrower than the experimental ones. The reason for this is that we model the excitation just as a change in partial charges of Trp, at fixed intramolecular geometry, which underestimates the effect of excitation on the equilibrium structure. However, the simulations correctly reproduce the experimentally observed narrowing of the band.

Figure 7A compares the local temperature of Trp (calculated from the average kinetic energy of the Trp atoms) with the square root of the variance of the simulated emission spectrum. It can be seen that there is a qualitatively similar behavior between the bandwidth profile (red) and the temperature profile (black), confirming the origin of the rise of the simulated spectra. The initial heating of the chromophores would result in the initial broadening, and the subsequent cooling down would contribute to the narrowing of the emission band. Furthermore, Figure 7B shows that the initial drop of the frequency shift due to intra-Trp interactions (IT component shown in Figure 6B) clearly follows the initial temperature rise (plotted in inverted scale, for better comparison). We rationalize these dynamics as a rapid IVR in the solute: IT contribution to the Stokes shift is due to a rearrangement of the COO^- and NH^{3+} groups as a response to the different charge distribution of the indole group in the ^1L_a state with respect to the ground state. There is a rapid decrease in potential energy of Trp (earliest frequency shift in Figure 6B), which results in an increase of the kinetic energy of Trp atoms, thus of the temperature (Figure 7). After this initial increase, there is a further, slower, decrease of the potential energy (slow red-shift in Figure 6B), but the temperature keeps decreasing because of a heat transfer to the environment (vibrational cooling). The simulated bandwidth profile is consistent with the experimental one. In particular, it is well fitted by a biexponentional function with the time constants of 450 fs and 7 ps found for experiment. Moreover, the experimental first moment M_1 tells us that after 5 ps the solvation dynamics are almost completely over, meaning that this 7 ps narrowing could not be solvation-driven or at most at a lower extent. These results support the interpretation of the time profile of the bandwidth in terms of IC/IVR and vibrational cooling.

The earlier (first 4 ps, Figure 7A) narrowing of the band is not only due to a decrease in temperature but also due to a strengthening of the solute−solvent interactions in the excited ^1L_a state. The bandwidth corresponding to $t = 0$ can be better estimated as the variance of the energy difference over the equilibrium 10 ns ground-state trajectory, which gives a value of ~910 cm^{-1} for ^1L_a. Similarly, the stationary emission bandwidth can be calculated from the equilibrium 10 ns ^1L_a trajectory, which gives 800 cm^{-1}. Therefore, there is an overall narrowing of the spectrum of 110 cm^{-1}, as measured by the square root of the variance. These bandwidths are calculated from equilibrium trajectories at constant (295 K) temperature. Therefore, this narrowing is not due to temperature variations but is rather evidence of the excited-state Trp−water interaction being stronger than in the ground state. Thus, the narrowing observed in Figures 4 and 6 has two origins: temperature transients due to IVR and vibrational cooling and an actual strengthening of the solute−solvent interaction.

Noteworthy is that in previous experimental studies of Trp fluorescence with lower time resolution and monochromatic detection, vibrational cooling was explicitly dismissed.[14,51] Although IVR and vibrational cooling are well-known phenomena that are noticeable when the excess vibrational energy is very high, of the order of hundreds of kelvin,[52,53] here we are able to detect an internal cooling by as little as 30 K, showing the sensitivity of the present experimental approach (also noted in other chromophores[20,22]).

A point to note is that both the strengthening of the interaction and the temperature transients should imply a breakdown of the linear response approximation (LRA) according to which[46]

$$\Delta\nu(t) \approx \frac{C_g(t)}{hk_BT} \approx \frac{C_e(t)}{hk_BT} \tag{13}$$

were h is Planck's constant, k_B is Boltzmann's constant, and $C_g(t)$ and $C_e(t)$ are the excitation energy correlation functions for the ground and excited states respectively. The LRA is usually assumed to be a good approximation for Trp. However, we shall see later that it cannot deal with some of the results reported in this work.

It is important to deal with this issue because without further consideration the LRA is frequently assumed. According to the LRA, the Stokes shift is related to the energy-difference autocorrelation function calculated either in the ground state or in the excited state. Replacing $t = 0$ into eq 13, we obtain

$$\Delta\nu(0) \approx \frac{C_g(0)}{hk_BT} \approx \frac{C_e(0)}{hk_BT} \tag{14}$$

where by definition $C_g(0) = \langle \Delta E^2 \rangle_g$ and $C_e(0) = \langle \Delta E^2 \rangle_e$ are variances of the initial $t = 0$ emission and stationary emission bands, respectively. As said before, for ^1L_a the "exact" static Stokes shift calculated with eq 4 is ~3870 cm^{-1}, whereas using eq 14, we obtain ~4050 and ~3130 cm^{-1} for the ground or excited correlation functions, respectively. In this way, we see that using the LRA with the ground-state correlation overestimates the total shift by ~10%, whereas with the excited-state one, it underestimates it by ~20%. These errors could and have been considered to be negligible in the sense that they are of the order of expected errors due to the approximate nature of the used theoretical force fields.[46] However, we stress that eq 14 implies that the initial and final bandwidths are expected to be the same. Moreover, implicit to eq 13 is the assumption of constant temperature throughout the relaxation process. We have shown before that none of these assumptions are valid. Therefore, even though for certain purposes the LRA can be used as a reasonable approximation, it cannot account qualitatively for aspects of the dynamics observed in this work, namely, the processes responsible for the variations of the emission bandwidth with time. Therefore, we think that equilibrium perturbative approximations are inadequate to deal with the detailed ultrafast spectral dynamics, as observed using the sensitive experimental techniques reported here, and that nonequilibrium theoretical treatments are unavoidable.

Conclusions

In summary, we presented UV broad-band fluorescence up-conversion measurements of tryptophan in bulk water with polarization detection and compared them with nonequilibrium MD simulations of ^1L_a and ^1L_b relaxation dynamics. The experimental and simulation results presented above allow us to draw the following conclusions:

(a) The time-resolved fluorescence anisotropy of tryptophan in water clearly exhibits a signature of an $^1L_b \rightarrow {}^1L_a$ IC in 45 ± 15 fs, confirming previous predictions.[8,14] Our observation of the wavelength dependence of the anisotropy provides evidence for emission from the ^1L_b state.

(b) The MD simulations confirm the biphasic relaxation of Trp in water with 160 fs and 1 ps exponential components. These times are attributed to collective motions and independent diffusion of several proximal water molecules.[27]

(c) We found a sub-10 fs decay that accounts for a ~1700 cm^{-1} shift of the total Stokes shift of 3800 cm^{-1}. The occurrence of sub-10 fs frequency shifts was recently observed on a variety of different systems.[19,20,22,29−32] Contrary to these systems, where such a fast Stokes shift is clearly intramolecular, we find here that the origin of this dynamics is intermolecular, i.e., due to solvation. It comes from the inertial motion of the water molecules and is associated with their independent rotational motion, as already predicted.[3]

(d) The broad-band detection provides reliable variance kinetics so that cooling dynamics can be sensitively followed. The excess vibrational energy, corresponding to a 30 K heating of the Trp, is responsible for ~6% of the final, thermalized, width and is released to the solvent in a biphasic way with 0.5 and 7 ps time constants. The former component could also take into account slower IVR processes among low frequency vibrational modes. In this respect, due to the concurrent effects of IC and IRF convolution the observed value of 0.5 ps could be slightly shorter. The different decay times found in the case of variance and first moment kinetics show that the latter are only solvation dynamics related. The most important result of the variance analysis is the experimental evidence of a ~50 fs rise corresponding to a broadening of 500 cm^{-1} (~30% of the thermalized width). This behavior is directly reflecting the IC process.

(e) The present study shows the sensitivity of femtosecond broad-band UV fluorescence up-conversion of Trp and is promising for its use in biological systems.

Acknowledgment. This work was supported by the Swiss National Science Fundation (FNS) via contract 200020-121839. J.E. is a researcher of CONICET. This work was partially supported by ANPYCT grant no. 1489/06.

Supporting Information Available: Raman and emission spectra. This material is available free of charge via the Internet at http://pubs.acs.org.

References and Notes

(1) Lakowicz, J. R. *Principles of fluorescence spectroscopy*; Plenum Press: New York, 1983.
(2) Beechem, J. M.; Brand, L. *Annu. Rev. Biochem.* **1985**, *54*, 43.
(3) Callis, P. R. *Fluorescence Spectrosc.* **1997**, *278*, 113.
(4) Vivian, J. T.; Callis, P. R. *Biophys. J.* **2001**, *80*, 2093.
(5) Callis, P. R.; Burgess, B. K. *J. Phys. Chem. B* **1997**, *101*, 9429.
(6) Lakowicz, J. R. *Photochem. Photobiol.* **2000**, *72*, 421.
(7) Schuler, B.; Eaton, W. A. *Curr. Opin. Struct. Biol.* **2008**, *18*, 16.
(8) Shen, X. H.; Knutson, J. R. *J. Phys. Chem. B* **2001**, *105*, 6260.
(9) Pal, S. K.; Peon, J.; Bagchi, B.; Zewail, A. H. *J. Phys. Chem. B* **2002**, *106*, 12376.
(10) Pal, S. K.; Peon, J.; Zewail, A. H. *Chem. Phys. Lett.* **2002**, *363*, 57.
(11) Peon, J.; Pal, S. K.; Zewail, A. H. *Proc. Natl. Acad. Sci. U.S.A.* **2002**, *99*, 10964.
(12) Pal, S. K.; Peon, J.; Zewail, A. H. *Proc. Natl. Acad. Sci. U.S.A.* **2002**, *99*, 1763.
(13) Zhang, L. Y.; Wang, L. J.; Kao, Y. T.; Qiu, W. H.; Yang, Y.; Okobiah, O.; Zhong, D. P. *Proc. Natl. Acad. Sci. U.S.A.* **2007**, *104*, 18461.
(14) Zhong, D. P.; Pal, S. K.; Zhang, D. Q.; Chan, S. I.; Zewail, A. H. *Proc. Natl. Acad. Sci. U.S.A.* **2002**, *99*, 13.
(15) Schenkl, S.; van Mourik, F.; van der Zwan, G.; Haacke, S.; Chergui, M. *Science* **2005**, *309*, 917.
(16) Leonard, J.; Portuondo-Campa, E.; Cannizzo, A.; van Mourik, F.; van der Zwan, G.; Tittor, J.; Haacke, S.; Chergui, M. *Proc. Natl. Acad. Sci. U.S.A.* **2009**, *106*, 7718.
(17) Zang, C.; Stevens, J. A.; Link, J. J.; Guo, L. J.; Wang, L. J.; Zhong, D. P. *J. Am. Chem. Soc.* **2009**, *131*, 2846.
(18) Stevens, J. A.; Link, J. J.; Kao, Y. T.; Zang, C.; Wang, L. J.; Zhong, D. P. *J. Phys. Chem. B* **2010**, *114*, 1498.
(19) Oskouei, A. A.; Bram, O.; Cannizzo, A.; van Mourik, F.; Tortschanoff, A.; Chergui, M. *J. Mol. Liq.* **2008**, *141*, 118.
(20) Oskouei, A. A.; Bram, O.; Cannizzo, A.; van Mourik, F.; Tortschanoff, A.; Chergui, M. *Chem. Phys.* **2008**, *350*, 104.
(21) Oskouei, A. A.; Tortschanoff, A.; Bräm, O.; van Mourik, F.; Cannizzo, A.; Chergui, M., *J. Chem. Phys*. **2010**, doi: 10.1063/1.3463448.
(22) Cannizzo, A.; Bram, O.; Zgrablic, G.; Tortschanoff, A.; Oskouei, A. A.; van Mourik, F.; Chergui, M. *Opt. Lett.* **2007**, *32*, 3555.
(23) Lu, W. Y.; Kim, J.; Qiu, W. H.; Zhong, D. P. *Chem. Phys. Lett.* **2004**, *388*, 120.
(24) Szabo, A. G.; Rayner, D. M. *J. Am. Chem. Soc.* **1980**, *102*, 554.
(25) Pal, S. K.; Peon, J.; Zewail, A. H. *Proc. Natl. Acad. Sci. U.S.A.* **2002**, *99*, 15297.
(26) Jarzeba, W.; Walker, G. C.; Johnson, A. E.; Kahlow, M. A.; Barbara, P. F. *J. Phys. Chem.* **1988**, *92*, 7039.
(27) Jimenez, R.; Fleming, G. R.; Kumar, P. V.; Maroncelli, M. *Nature* **1994**, *369*, 471.
(28) Vengris, M.; van der Horst, M. A.; Zgrablic, G.; van Stokkum, I. H. M.; Haacke, S.; Chergui, M.; Hellingwerf, K. J.; van Grondelle, R.; Larsen, D. S. *Biophys. J.* **2004**, *87*, 1848.
(29) Cannizzo, A.; van Mourik, F.; Gawelda, W.; Zgrablic, G.; Bressler, C.; Chergui, M. *Angew. Chem., Int. Ed.* **2006**, *45*, 3174.
(30) Gawelda, W.; Cannizzo, A.; Pham, V. T.; van Mourik, F.; Bressler, C.; Chergui, M. *J. Am. Chem. Soc.* **2007**, *129*, 8199.
(31) Zgrablic, G.; Voitchovsky, K.; Kindermann, M.; Haacke, S.; Chergui, M. *Biophys. J.* **2005**, *88*, 2779.
(32) Zgrablic, G.; Haacke, S.; Chergui, M. *J. Phys. Chem. B* **2009**, *113*, 4384.
(33) Bräm, O.; ElNahhas, A.; Cannizzo, A.; Chergui, M. *Chem. Phys. Lett.* **2010**, submitted.

(34) Hansen, J. E.; Rosenthal, S. J.; Fleming, G. R. *J. Phys. Chem.* **1992**, *96*, 3034.
(35) Ruggiero, A. J.; Todd, D. C.; Fleming, G. R. *J. Am. Chem. Soc.* **1990**, *112*, 1003.
(36) Hare, D. E.; Sorensen, C. M. *J. Chem. Phys.* **1990**, *93*, 25.
(37) Lindahl, E.; Hess, B.; van der Spoel, D. *J. Mol. Model.* **2001**, *7*, 306.
(38) Daura, X.; Suter, R.; van Gunsteren, W. F. *J. Chem. Phys.* **1999**, *110*, 3049.
(39) Mark, P.; Nilsson, L. *J. Phys. Chem. B* **2002**, *106*, 9440.
(40) Hassanali, A. A.; Li, T. P.; Zhong, D. P.; Singer, S. J. *J. Phys. Chem. B* **2006**, *110*, 10497.
(41) Li, T. P.; Hassanali, A. A. P.; Kao, Y. T.; Zhong, D. P.; Singer, S. J. *J. Am. Chem. Soc.* **2007**, *129*, 3376.
(42) Darden, T.; York, D.; Pedersen, L. *J. Chem. Phys.* **1993**, *98*, 10089.
(43) Essmann, U.; Perera, L.; Berkowitz, M. L.; Darden, T.; Lee, H.; Pedersen, L. G. *J. Chem. Phys.* **1995**, *103*, 8577.
(44) Hess, B.; Bekker, H.; Berendsen, H. J. C.; Fraaije, J. G. E. M. *J. Comput. Chem.* **1997**, *18*, 1463.
(45) Sobolewski, A. L.; Domcke, W. *Chem. Phys. Lett.* **1999**, *315*, 293.
(46) Nilsson, L.; Halle, B. *Proc. Natl. Acad. Sci. U.S.A.* **2005**, *102*, 13867.
(47) Berendsen, H. J. C.; Postma, J. P. M.; Vangunsteren, W. F.; Dinola, A.; Haak, J. R. *J. Chem. Phys.* **1984**, *81*, 3684.
(48) Dashnau, J. L.; Zelent, B.; Vanderkooi, J. M. *Biophys. Chem.* **2005**, *114*, 71.
(49) Muino, P. L.; Callis, P. R. *J. Chem. Phys.* **1994**, *100*, 4093.
(50) Shen, X. H.; Knutson, J. R. *Chem. Phys. Lett.* **2001**, *339*, 191.
(51) Qiu, W. H.; Zhang, L. Y.; Kao, Y. T.; Lu, W. Y.; Li, T. P.; Kim, J.; Sollenberger, G. M.; Wang, L. J.; Zhong, D. P. *J. Phys. Chem. B* **2005**, *109*, 16901.
(52) Henry, E. R.; Eaton, W. A.; Hochstrasser, R. M. *Proc. Natl. Acad. Sci. U.S.A.* **1986**, *83*, 8982.
(53) Okazaki, I.; Hara, Y.; Nagaoka, M. *Chem. Phys. Lett.* **2001**, *337*, 151.

JP101778U